Jurnal Penelitian Fisika dan Aplikasinya (JPFA) *Volume 11, Issue 02, December 2021*
p-ISSN: 2087-9946 DOI: 10.26740/jpfa.v11n2.p148-157
e-ISSN: 2477-1775 https://journal.unesa.ac.id/index.php/

Research Article

Microstructure and Optical Properties Study of Nd-doped $BiFeO_3$ ($Ba_{1-x}Nd_xFeO_3$) Films on Quartz Substrate

Yofentina Iriani[1,a,*], Dianisa Khoirum Sandi[1,b] , Rainisa Nurmawanti[1,c], Sri Budiawanti[2,d], Elvinda Bendra Agustina[1,3,e]

[1]Physics Department, Sebelas Maret University, Surakarta, Indonesia
[2] Physics Education Department, Sebelas Maret University, Surakarta, Indonesia
[3]Institut Teknologi dan Sains Nahdlatul Ulama, Pekalongan, Indonesia

e-mail: [a]yofent_iriani@staff.uns.ac.id, [b]dianisa875@gmail.com, [c]rnurmawanti@gmail.com, [d]sribudiawanti@staff.uns.ac.id and [e]elvindabendra@itsnupekalongan.ac.id
* Corresponding Author

Abstract

*Bismuth ferrite oxide (BFO), due to its remarkable properties, has become one of the most attractive multiferroic materials to be extensively studied. BFO doped with various materials, including Neodymium (Nd), could improve its properties that apply to numerous electronic devices. However, the studies related to the properties of Nd-doped BFO (**$Ba_{1-x}Nd_xFeO_3$**) thin films on a quartz substrate, especially the optical properties, are relatively scarce. This study aimed to investigate the microstructure and optical properties of the Nd-doped BFO (BNFO) as the variation of the Nd concentrations. The BNFO thin films with Nd concentrations of 0.05 (BNFO5); 0.1 (BNFO10); and 0.2 (BNFO20) have been deposited on the quartz substrates via the sol-gel method and using spin coating. The films were annealed at 600 °C for 1.5 h. The XRD result of the BNFO films revealed a single phase of BFO with a cubic structure. The lattice constants and volume cells of the films declined with more Nd. Meanwhile, the crystallite size and lattice strain changed due to the change in the Nd number. Additionally, the morphology images showed the pores on the films' surface and the different film thicknesses of each BNFO film. From the optical characterization, the transmittance spectra of the BNFO films tended to rise as the more Nd amount doped, in which the BNFO20 had the highest transmittance. The BNFO10 had the highest refractive index, followed by the BNFO5 and BNFO20. Contrarily, the BNFO20 had the highest extinction coefficient and $(n^2-1)^{-1}$ spectra, followed by the BNFO5 and BNFO10. Further, the bandgap values of the BNFO5, BNFO10, and BNFO20 were 2.75, 2.85, and 2.64 eV, respectively. Accordingly, due to the highest Nd amount that most impacted its microstructure, the BNFO20 exhibited the lowest bandgap value compared to the other films that are good for photovoltaic applications.*

Keywords: *$Ba_{1-x}Nd_xFeO_3$ thin films; quartz substrate; sol-gel method; microstructure property; optical property*

Jurnal Penelitian Fisika dan Aplikasinya (JPFA), 2021; **11**(2): 148-157

Studi Sifat Mikrostruktur dan Sifat Optik Lapisan $BiFeO_3$ doping Nd ($Ba_{1-x}Nd_xFeO_3$) diatas Substrat Kuarsa

Abstrak

Bismut ferit oksida (BFO) adalah salah satu material multiferroik yang paling menarik yang telah dipelajari secara ekstensif karena sifatnya yang luar biasa. BFO yang didoping beberapa bahan termasuk salah satunya Neodymium (Nd) dapat meningkatkan sifat BFO sehingga dapat diterapkan di berbagai perangkat elektronik. Namun, studi terkait sifat-sifat lapisan tipis BFO yang didoping Nd pada substrat kuarsa terutama sifat optiknya masih jarang ditemukan. Penelitian ini bertujuan untuk mempelajari mikrostruktur dan sifat optik lapisan BFO yang didoping Nd (BNFO or $Ba_{1-x}Nd_xFeO_3$) sebagai akibat dari variasi konsentrasi Nd. Dalam studi ini, lapisan tipis BNFO dengan konsentrasi Nd sebesar x=0.05 (BNFO5); 0.1 (BNFO10); and 0.2 (BNFO20) telah dibuat diatas substrat kuarsa menggunakan metode sol gel dengan spin coater. Lapisan tersebut diannealing pada suhu 600 °C selama 1.5 jam. Hasil pola XRD lapisan tipis BNFO menunjukkan fase tunggal BFO dengan struktur kubus. Konstanta kisi dan volume sel lapisan BNFO semakin menurun seiring dengan semakin banyaknya Nd. Sedangkan ukuran kristal dan regangan kisi berubah karena jumlah Nd berubah. Selain itu, gambar morfologi permukaan menunjukkan adanya pori-pori pada permukaan lapisan dan ketebalan yang berbeda pada setiap lapisan tipis BNFO. Dari karaterisasi optik, spektrum transmitansi dari lapisan BNFO cenderung meningkat seiring banyaknya dopan Nd yang mana lapisan BNFO20 memiliki nilai transmitansi tertinggi. Lapisan BNFO10 memiliki indeks bias tertinggi diikuti oleh lapisan BNFO5 dan BNFO20. Sebaliknya, BNFO20 memiliki koefisien extiction dan spektrum $(n^2-1)^{-1}$ tertinggi diikuti oleh BNFO5, dan BNFO10. Selanjutnya, nilai bandgap dari BNFO5, BNFO10 dan BNFO20 masing-masing adalah 2.75, 2.85, dan 2.64 eV. Dengan demikian, karena konsentrasi Nd tertinggi yang paling berdampak pada mikrostrukturnya, BNFO20 memiiki nilai bandgap terendah dibandingkan dengan lapisan-lapisan lainnya, sehingga bagus untuk aplikasi fotovoltaik.

Kata Kunci: *Lapisan tipis $Ba_{1-x}Nd_xFeO_3$; substrat kuarsa; metode sol gel; sifat mikro; sifat optik*

PACS: 78.66.-w; 81.40.-z

Article History: Received: 4 March 2021 Approved with minor revision: 14 November 2021
Accepted: 12 December 2021 Published: 30 December 2021

How to cite: Iriani Y, et al. Microstructure and Optical Properties Study of Nd-doped $BiFeO_3$ ($Ba_{1-x}Nd_xFeO_3$) Films on Quartz Substrate. *Jurnal Penelitian Fisika dan Aplikasinya (JPFA)*. 2021; **11**(2): 148-157. DOI: https://doi.org/10.26740/jpfa.v11n2.p148-157.

I. INTRODUCTION

Multiferroic materials have been fascinating in the studies of multifunctional materials. It is a material possessing ferroic properties of ferroelasticity, ferroelectricity, and antiferromagnetism [1-3]. It reveals potential applications in electronic devices such as sensors, photovoltaics [4,5], spintronics [6], photoelectrochemicals [3], photocatalysts, or element memory [2,7,8]. Bismuth Ferrite ($BiFeO_3$ or BFO) has become one of the most promising multiferroic materials, intensively studied due to its remarkable properties. It has rhombohedral distorted ABO_3 (A-site is Bi^{3+} and B-site is Fe^{2+}) perovskite crystal structures with *R3c* space group [9]. It is the only multiferroic material that possesses ferroelectric with

Currie temperature (T_C = 825 °C) and antiferromagnetism with Neel temperature (T_N = 370 °C) [3,7,8,10]. BFO is a Pb-free multiferroic material with large saturation polarization and a small energy bandgap (2.1-2.7 eV) [2-4]. Moreover, it has been demonstrated that BFO thin films have high remanent polarization and low magnetization intensity [4,8,11]. However, in the presence of Fe^{2+} and oxygen vacancies, BFO is susceptible to high leakage current [1,10,12,13]. Additionally, BFO thin films own a low dielectric constant and low electric resistivity [8,14]. These drawbacks limit the multifunctional applications of BFO.

Modifying BFO by doping is the most effective approach to resolve these matters and enhance its ferroelectric and magnetic properties [9,12,14,15]. To increase ferromagnetic and ferroelectric properties, the rare-earth (RE) dopants (La, Nd, Gd, Er, Dy, Eu, Sm) have been applied in BFO, which are isovalently substituted by the A-site (Bi^{3+}) [5,7,16,17]. The replacement of the Bi-site can reduce the oxygen vacancies by adjusting the volatility of Bi atoms and thus increase photovoltaic properties [13].

Chang et al. reported that Nd doping in Bi sites of BFO ceramics could decrease the FeO_6 octahedral distortion by increasing the anisotropy of Bi/Nd-O bonds, which declined leakage current [7,9]. Ukai et al. exposed that Nd substitution in the Bi sites reduced the Bi deficiency and improved photovoltaic properties [4]. Moreover, there have been many studies that reported the Nd-doped BFO films deposited on (111) Pt/Ti/SiO_2/Si [10], and transparent FTO [8,11], ITO [13], SRO [3], LAO [17] substrates. Also, among the available methods, thin film manufactured by a chemical solution deposition (CSD) or sol-gel method [18-21] has potential advantages: easy operation, low cost, high purity, and low heating temperature. However, few works have concerned Nd-doped BFO thin films with various doping levels deposited on transparent quartz substrates. Therefore, this study presents the report of the fabrication of BFO-doped various Nd on the quartz substrate by the sol-gel method. The objective is to investigate the effects of Nd concentrations on the properties of the BFO and Nd-doped BFO thin films with potential advantages for photovoltaic purposes.

II. METHOD

In this study, the thin films of Nd-doped BFO with the formula of $Bi_{1-x}Nd_xFeO_3$ (x = 0.05, x = 0.1, and x = 0.2) were fabricated on quartz substrates via the sol-gel method. The precursors were Bismuth (III) Nitrate $[Bi(NO_3)_3].5H_2O$ (Sigma Aldrich, ≥ 99%), Ferrite Nitrate $[Fe(NO_3)_3].9H_2O$ (Sigma Aldrich, ≥ 99%), and Neodymium Nitrate $[Nd(NO_3)_3].6H_2O$ (Sigma Aldrich, ≥ 99%) as the Bi, Fe, and Nd sources; while Acetic Acid (CH_3COOH) (Sigma Aldrich, ≥ 99.7%) and 2-methoxyetanol ($C_3H_8O_2$) (Sigma Aldrich, ≥ 99.8%) were as the solvents; and acetylacetone was as a stabilizing agent. The solutions of $Bi_{1-x}Nd_xFeO_3$ were deposited on the substrates using a spin coater with a spin rate of 3000 rpm for 3 min. The films were then annealed in a furnace with a temperature of 600 °C and a holding time of 1.5 h.

The films were denoted by BNFO5, BNFO10, and BNFO20 for the BFO doped Nd with x=0.05, x=10, and x=20, respectively. The structural properties of BNFO films were analyzed using an X-ray diffraction (XRD) Shimadzu7000 instrument. The morphology and thickness of the films were determined through a scanning electron microscope (SEM) Hitachi SU3500 instrument. Meanwhile, the optical properties were examined via a UV-Vis spectrophotometer Perkin Elmer Lambda25.

III. RESULTS AND DISCUSSION

Figure 1 shows the XRD patterns of the BNFO thin films with the enlargement of (101) planes on the right side. The patterns validate a single phase of the orthorhombic $BiFeO_3$ crystal structure corresponding to ICDD number #742016 with $a = b = c$ and $\alpha = \beta = \gamma = 89.400°$, and *R3m* space group. Also, the patterns exhibit no impurity peaks, and no second phase was observed. Almost all peaks shift towards the higher 2θ values as the higher Nd dopant concentration indicates a change in the lattice constants of the BFNO films in Table 1.

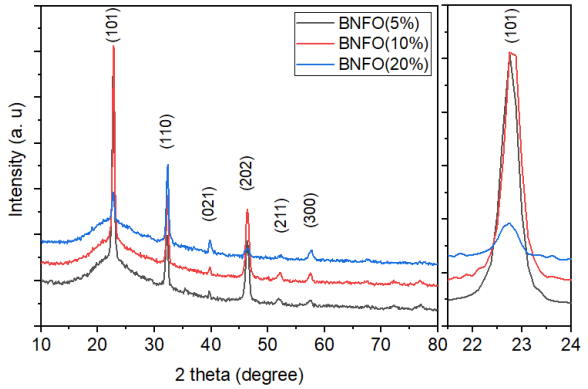

Figure 1. XRD Patterns of the BNFO thin films

The lattice constants are gradually decrease with an increase in the Nd dopant amount. This indicates the replacement of Nd^{2+} ions in the Bi^{3+} ions site within the BFO crystal site. The substituted Nd^{2+} ionic radii (1.109 Å) are smaller than that of the host Bi^{3+} (1.170 Å) ions, so it causes the reduction of the lattice constants and, thus, in the volume cell. The crystallite size of the BNFO films was obtained by manual calculation using the modified Scherer equation [22]. The crystallite size is smaller with the rise of Nd dopant amount, associated with the lattice constants due to the smaller dopant Nd than the host Bi. Here, the crystallite size of BNFO20 significantly decreases because it receives the most Nd dopant. The lattice is attained by manual calculation through the William-Hall analysis. The strain is found to be in similar values but gradually decreases with more Nd. The declining strain confirms the stability of the structure as the higher dopant concentration in the lattice [23].

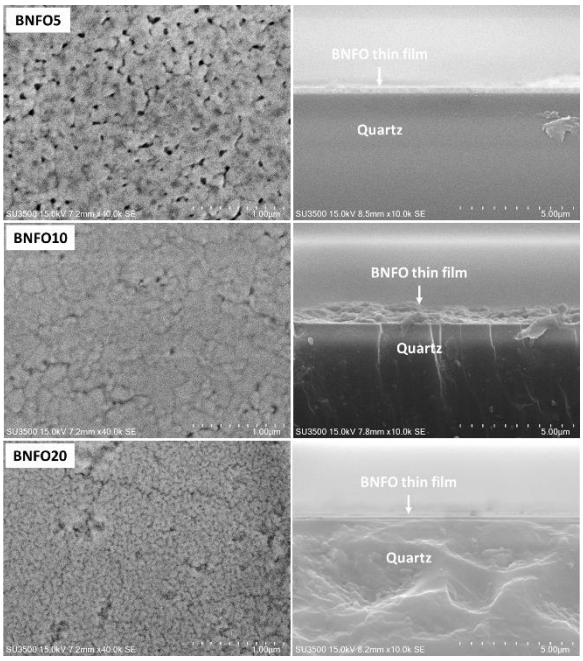

Figure 2. Morphology and cross-section images of BNFO thin films

Figure 2 presents the morphology and cross-sectional images of BNFO thin films. As shown, the grains of all BNFO samples appear fused. However, it seems that the particle size of the samples becomes smaller or finer as the more Nd dopant. This phenomenon correlates with the XRD results, especially on the crystallite size and cell volume, where the values also decrease due to the increasing Nd amount. Furthermore, all films show the formation of pores, especially on BNFO5 and BNFO10, while BNFO20 appears to have microcracks on the surface. Next, the thicknesses of the BNFO films have been estimated from the cross-section images listed in Table 2. It is known that the BNFO10 is very thick as compared to the others, which may influence the optical properties.

Table 1. Structural properties of BNFO thin films

Samples	Crystallite size (nm)	Lattice Constants (Å)	Volume cell (Å ^{3})	Lattice Strain
BNFO5	215.072	3.930	60.679	0.0064
BNFO10	211.594	3.921	60.282	0.0063
BNFO20	160.882	3.916	60.053	0.0058

Table 2. The thickness of the BNFO thin films

Samples	Thickness (nm)
BNFO5	277
BNFO10	469
BNFO20	144

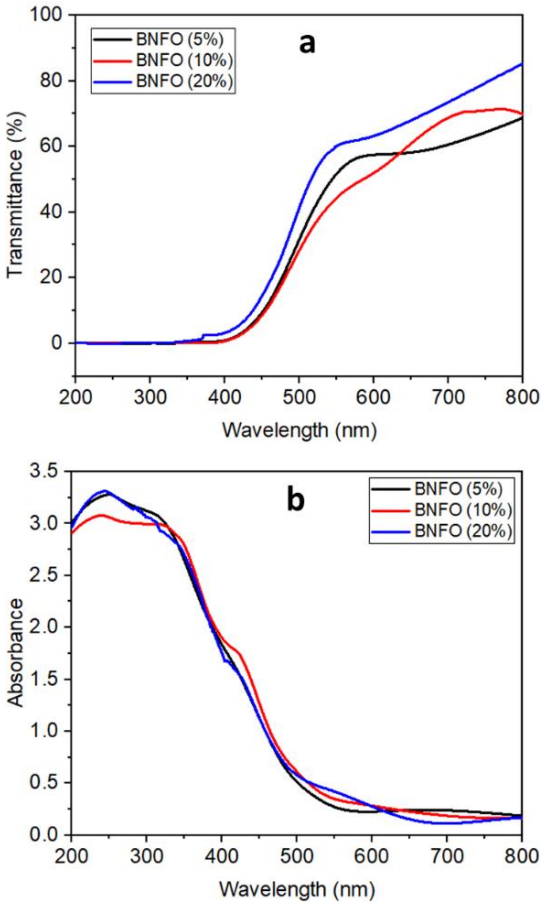

Figure 3. (a) The absorbance and (b) The transmittance spectra of the BNFO thin films

Figures 3a and 3b demonstrate the absorbance and transmittance spectra of the BNFO thin films in the 200-800 nm wavelength range. It can be seen that more Nd doping upsurges the transmittance spectra of the films. However, the absorbance values are overlapped even with the variation of the Nd concentrations except for the BNFO10, which has the lowest peak. Surprisingly, even though the BNFO20 has the highest transmittance values, the absorbance peak also presents the highest. Nevertheless, all films start to absorb the amount of light before the visible region (at a wavelength below 550 nm). It is reported by Xue et al. [11] that the absorption bands, which are at around 500 nm, may be attributed to an electronic transition.

Furthermore, the absorption edges move slightly toward a lower wavelength with the rise in the Nd concentrations. This points to the change in the electronic structure of the BNFO film [11,24]. It also indicates the modification of the bandgap values of the films [25].

Through the transmittance data and film thickness, the refractive index (n), extinction coefficient (k), dispersion energy ($1/(n^2-1)$), and bandgap values (Eg) could be achieved. The refractive index of the various Nd-doped films was computed using Swanepoel's method [26,27]. Figure 4a shows the refractive index dispersion spectra of the BNFO thin films at 400-700 nm.

Many reported that the refractive index falls at a higher wavelength. The refractive index values of the films are in the range of 2.8-1.7. The BNFO10 (x=0.1) has the highest refractive index, while at the BNFO of x=0.05 and x=0.2, the refractive index reduces as the

more Nd content. It is mentioned that the refractive index may depend on the films' lattice contraction, stoichiometry, and packing density [28].

The extinction coefficient is inversely proportional to the refractive index. The extinction coefficient describes how much incident light is reduced or lost compared to the light energy on the surface due to the absorption and scattering processes. Figure 4b presents the extinction coefficient of the BNFO thin films as a function of the wavelength. The extinction coefficient is obtained from $k = \alpha\lambda/4\pi$, which α is the absorption coefficient [25]. Based on Figure 4b, the extinction coefficient increases with the shorter wavelength and is sharply below 550 nm (in the high absorbance spectra). It is observed that the BNFO20 has the highest extinction coefficient, which indicates that this film can strongly absorb light as compared to the others.

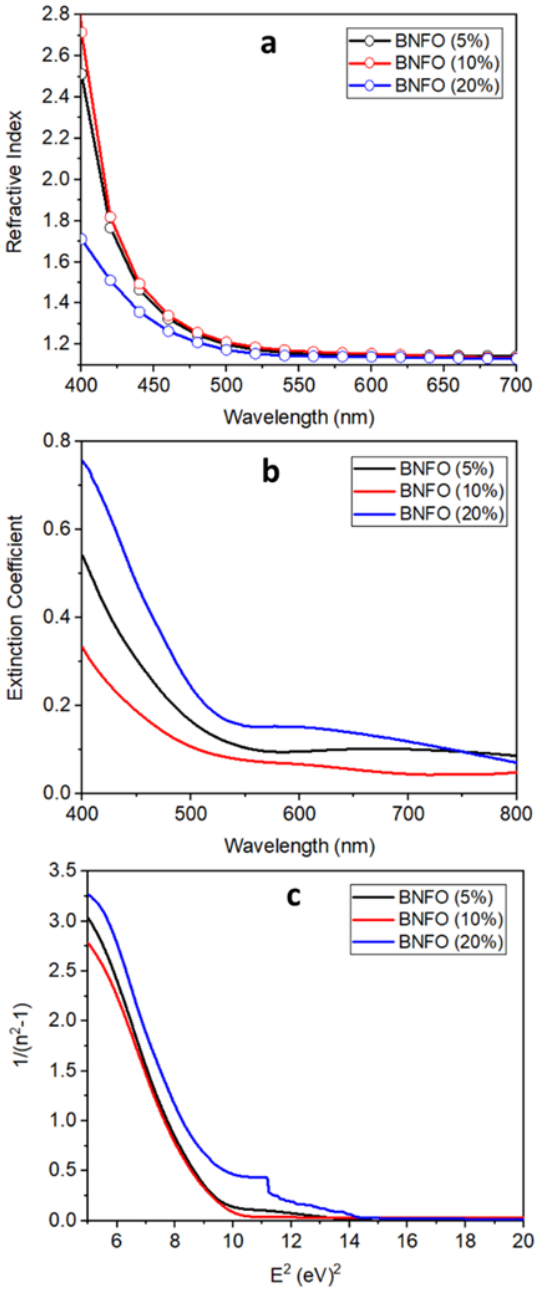

Figure 4. (a) The refractive index, (b) The extinction coefficient, and (c) The plot of $1/(n^2-1)$ vs E^2 of the BNFO thin films

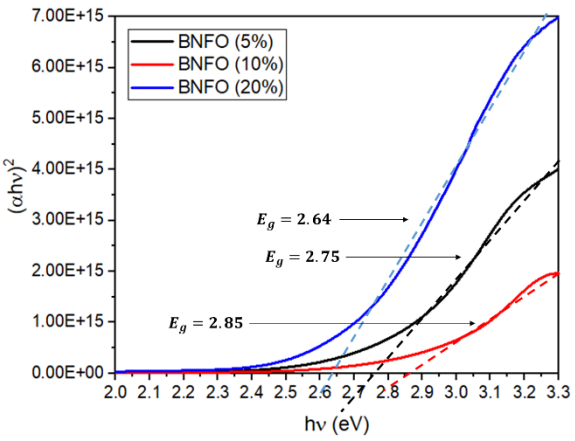

Figure 5. Tauc's plot for the BNFO thin films

Wemple et al. [29, 30] examined the strong dispersion of the refractive index exhibited below the absorption edge using the single oscillator model. Based on the model, the dependence of the refractive index on the photon energy can be plotted to the Wemple-DiDomenico relationship, as shown in Figure 4c. In Figure 3c, the refractive index is expressed by $(n^2-1)^{-1} = \frac{E_o}{E_d} - \left(\frac{1}{E_o E_d}\right) E^2$ where E_o is the single oscillator energy, E_d is the disperse energy, and E^2 is the photons' energy [30]. From Figure 3c, the $(n^2-1)^{-1}$ spectra are influenced by the Nd doping.

The BNFO is a direct bandgap material [11], and the optical bandgap value (Eg) can be found in Tauc's plot, which is the curve of $(\alpha h\nu)^2$ vs $h\nu$ shown in Figure 5. The linear extrapolation from the plot gives the films an optical bandgap.

The change in the bandgap values may be attributed to the lattice distortion, electronic band structure, oxygen vacancies, grain size, and defect conditions [24,31]. Further, the Eg increases with reducing crystallite size and film thickness due to quantum size effects in nanocrystalline films [24,28]. Thus, the Eg should be wider as the higher Nd concentration is given because the results exhibit that more Nd dopant leads to smaller crystallite size and cell volume.

However, from the figure, the bandgap values increase along with the more Nd content for the BNFO of x=0.05 and x=0.1. Meanwhile, the BNFO20 (x=0.2) has the lowest bandgap values, which are inappropriate for the theory mentioned. For this reason, it might be associated that more dopants will lead to higher lattice distortion that can adjust the micro-strain in the doped BFO structure and thus enhance the absorption in the visible region [24]. Besides, the higher doping may lead to more defects such as oxygen vacancies or holes between valence and conduction band edge, thus narrowing the band gap [24,31]. On the other hand, the bandgap value may also depend on the film thickness.

This research is still limited to the optical properties of Nd-doped BFO. The application of this material is for photovoltaics, so the characterization of electrical properties to determine diode behavior is to be done further.

IV. CONCLUSION

The growth of the Nd-doped BFO thin films on the quartz substrates has been conducted via the sol-gel method prepared by a spin coater. The XRD patterns confirm that the BNFO films are a single phase with an orthorhombic structure. The lattice constants, volume cell, and lattice constants of the BNFO films reduce as the Nd amount increases. The surface morphology images show that the films have pores with different thickness values for each BNFO thin film. The transmittance spectra of the BNFO films tend to rise as the more Nd dopant, while the absorbance spectra overlap with the BNFO20, which has the highest transmittance value and absorbance. The BNFO10 film has the highest refractive index, followed by the BNFO5 and BNFO20 films. Contrarily, the BNFO20 has the highest extinction coefficient and $(n^2-1)^{-1}$ spectra, followed by the BNFO5 and

BNFO10. As a result, due to the most Nd amount, the BNFO20 reveals the lowest bandgap value compared to the other films, which is suitable for photovoltaic applications in the future.

ACKNOWLEDGMENT

The authors wish to thank *Penelitian Unggulan Terapan* 2020 PNBP UNS No. 452/UN27.21/PP/2020 for the financial support.

REFERENCES

[1] Tomczyk M, Stroppa DG, Reaney IM and Vilarinho PM. Growth of BiFeO3 thin films by chemical solution deposition: the role of electrodes. *Physical Chemistry Chemical Physics*. 2017; **19**(22); 14337-14344. DOI: https://doi.org/10.1039/C7CP01842H.

[2] Maleki H, Falahatnezhad S and Taraz M. Influence of Thickness on the Structural, Optical and Magnetic Properties of Bismuth Ferrite Thin Films. *Journal of Superconductivity and Novel Magnetism*. 2018; **31**(10); 3217-3222. DOI: https://doi.org/10.1007/s10948-018-4584-0.

[3] Tan KH, Chen YW, Van CN, Wang H, Chen JW, Lim FS, Chew KH, Zhan Q, Wu CL, Chai SP, Chu YH and Chang WS. Energy Band Gap Modulation in Nd-doped BiFeO3/SrRuO3 Heteroepitaxy for Visible Light Photoelectrochemical Activity, *ACS Applied Materials and Interfaces*. 2019; **11**(1); 1655-1664. DOI: https://doi.org/10.1021/acsami.8b17758

[4] Ukai Y, Yamazaki S, Kawae T and Morimoto A. Polarization-Induced Photovoltaic Effects in Nd-Doped $BiFeO_3$ Ferroelectric Thin Films. *Japanese Journal of Applied Physics*. 2012; **51**(9S1); 09LE10. DOI: https://doi.org/10.1143/JJAP.51.09LE10.

[5] Shi T, Wang J, Yan W, Shao X and Hou ZL. Enhanced photovoltaic property based on reduced leakage current and band gap in Nd-doped $BiFeO_3$ films. *Materials Research Express*. 2018; **6**(8); 086426. DOI: https://doi.org/10.1088/2053-1591/ab1b8b.

[6] Zhang HR, Kalantari K, Marincel DM, Trolier-McKinstry S, MacLaren I, Ramasse QM, Rainforth W and Reaney IM. The effect of substrate clamping on the paraelectric to antiferroelectric phase transition in Nd-doped $BiFeO_3$ thin films. *Thin Solid Films*. 2016; **616;** 767-772. DOI: https://doi.org/10.1016/j.tsf.2016.10.004.

[7] Zhang Y, Wang Y, Qi J, Tian Y, Sun M, Zhang J, Hu T, Wei M, Liu Y and Yang J. Enhanced Magnetic Properties of $BiFeO_3$ Thin Films by Doping: Analysis of Structure and Morphology. *Nanomaterials.* 2018; **8**(9); 711. DOI: https://doi.org/10.3390/nano8090711.

[8] Meng C, Guoqiang T, Xu X, Ao X and Huijun R. Preparation of Nd-doped BiFeO3 films and their electrical properties. *Physica B: Condensed Matter.* 2012; **407**(17) 3360-3363. DOI: https://doi.org/10.1016/j.physb.2012.04.038.

[9] Zhang J, Ma P, Shi T and Shao X. Nd-Cr co-doped $BiFeO_3$ thin films for photovoltaic devices with enhanced photovoltaic performance. *Thin Solid Films*. 2020; **698**; 137852. DOI: https://doi.org/10.1016/j.tsf.2020.137852.

[10] Thang DV, Oanh LTM, Khang NC, Hung NM, Bich DD, Thao DTX and Minh NV, Structural, magnetic and electric properties of Nd and Ni co-doped $BiFeO_3$ materials. *AIMS Materials Science*. 2017; **4**(4); 982-990. DOI: https://doi.org/10.3934/matersci.2017.4.982.

[11] Xue X, Tan G, Liu W and Hao H. Study on pure and Nd-doped BiFeO3 thin films prepared by chemical solution deposition method. *Journal of Alloys and Compounds*. 2014; **604**; 57-65. DOI: https://doi.org/10.1016/j.jallcom.2014.03.122.

[12] Li X, Wang X, Li Y, Mao W, Li P, Yang T,

and Yang J. Structural, morphological and multiferroic properties of Pr and Co co-substituted $BiFeO_3$ nanoparticles. *Materials Letters.* 2013; **90**; 152-155. DOI: https://doi.org/10.1016/j.matlet.2012.09.038.

[13] Peng YT, Chiou SH, Hsiao CH, Ouyang CH, and Tu C. Remarkably enhanced photovoltaic effects and first-principles calculations in neodymium doped $BiFeO_3$. *Scientific Reports*. 2017; **7;** 45164. DOI: https://doi.org/10.1038/srep45164.

[14] Bai L, Sun M, Ma W, Yang J, Zhang J, and Liu Y. Enhanced Magnetic Properties of Co-Doped BiFeO3 Thin Films via Structural Progression. *Nanomaterials.* 2020; **10**; 1798. DOI: https://doi.org/10.3390/nano10091798.

[15] Ma Z, Liu H, Wang L, Zhang F, Zhu L, and Fan S. Phase transition and multiferroic properties of Zr-doped $BiFeO_3$ thin films. *Journal of Materials Chemistry C*. 2020; **8**(48); 17307-17317. DOI: https://doi.org/10.1039/D0TC04593D.

[16] Chang WS, Tu CS, Chen PY, Chen CS, Lin CY, Feng KC, Hsieh YL, and Huang YH. Effects of Fe 3d–O 2p and Bi 6sp–O 2p orbital hybridizations in Nd doped $BiFeO_3$ ceramics. *Journal of Alloys and Compounds.* 2017; **710**; 670-679. DOI: https://doi.org/10.1016/j.jallcom.2017.03.329.

[17] Huong NT, Lee S, Atabaev TS, Kurisu M, and Hong NH. Rare Earth-Doped BiFeO3Thin Films: Relationship between Structural and Magnetic Properties. *Advances in Condensed Matter Physics.* 2015; **2015**; 371802. DOI: https://doi.org/10.1155/2015/371802.

[18] Iriani Y, Megasari NH, and Nurosyid F. Pengaruh Suhu Annealing terhadap Struktur Mikro dan Sifat Optik Lapisan Bismuth Ferrite ($BiFeO_3$). I*ndonesian Journal of Applied Physics.* 2019; **9**(1); 41-45. DOI: https://doi.org/10.13057/ijap.v9i01.33262.

[19] Shirahata Y and Takeo O. Characterization and Photovoltaic Properties of $BiFeO_3$ Thin Films. *Coatings*. 2016; **6**(4); 68. DOI: https://doi.org/10.3390/coatings6040068.

[20] Santika M, Iriani Y, and Suryana R. Influence of Thickness on Optical Properties of Bismuth Ferrite Layers Grown on Quartz Substrates by Chemical Solution Deposition. *Materials Today: Proceedings.* 2019; **13**(1); 82-86. DOI: https://doi.org/10.1016/j.matpr.2019.03.192.

[21] Agustina EB, Iriani Y, and Suryana R. Effect of Pre-Annealing and Annealing Temperature on Microstructural and Optical Properties of Multiferroic $BiFeO_3$ Thin Films Prepared by Chemical Solution Deposition (CSD). *Journal of Physics: Conference Series*. 2019; **1397**; 012002. DOI: https://doi.org/10.1088/1742-6596/1397/1/012002.

[22] Monshi A, Foroughi MR, and Monshi MR. Modified Scherrer Equation to Estimate More Accurately Nano-Crystallite Size Using XRD. *World Journal of Nano Science and Engineering*. 2012; **2**(3); 154-160. DOI: https://doi.org/10.4236/wjnse.2012.23020.

[23] Kumari A, Kumari K, Ahmed F, Alshoaibi A, Alvi PA, Dalela S, Ahmad MM, Aljawfi RN, Dua P, Vij A, and Kumar S. Influence of Sm Doping on Structural, Ferroelectric, Electrical, Optical and Magnetic Properties of $BaTiO_3$. *Vacuum*. 2021; **184**; 109872. DOI: https://doi.org/10.1016/j.vacuum.2020.109872.

[24] Deng X, Zeng Z, Gao R, Wang Z, Chen G, Cai W, and Fu C. Study of Structural, Optical and Enhanced Multiferroic Properties of Ni Doped BFO Thin Films Synthesized By Sol-Gel Method. *Journal of Alloys and Compounds.* 2020; **831**; 154857. DOI: https://doi.org/10.1016/j.jallcom.2020.154857.

[25] Ranjbar S, Ranjbar A, Behdani M, and Roknabadi MR. Fabrication of Bismuth Titanate ($Bi_4Ti_3O_{12}$) Thin Films: Effect of Annealing Temperature on their Structural

and Optical Properties. *Scientia Iranica*. 2018; **26**(3); 1990-1996. DOI: https://doi.org/10.24200/sci.2018.51061.1992.

[26] Swanepoel R. Determination of The Thickness and Optical Constants of Amorphous Silicon. *Journal of Physics E: Scientfic Instruments.* 1983; **16**(12); 1214-1222. DOI: https://doi.org/10.1088/0022-3735/16/12/023.

[27] Swanepoel R. Determination of Surface Roughness and Optical Constants of Inhomogeneous Amorphous Silicon Films. *Journal Physics E: Scientific Instruments.* 1984; **17**(10); 896-903. DOI: https://doi.org/10.1088/0022-3735/17/10/023.

[28] Sharma HB. Structural and Optical Properties of Sol-Gel Derived Barium Titanate Thin Film. *International Journal of Modern Physics B.* 2007; **21**(11); 1837–1849. DOI: https://doi.org/10.1142/S0217979207037028.

[29] Wemple SH and DiDomenico M. Optical Dispersion and the Structure of Solids. *Physical Review Letters*. 1969; **23**(20); 1156-1160. DOI: https://doi.org/10.1103/PhysRevLett.23.1156.

[30] Wemple SH and DiDomenico M. Behavior of the Electronic Dielectric Constant in Covalent and Ionic Materials. *Physical Review B*. 1971; **3**(4); 1338-1351. DOI: https://doi.org/10.1103/PhysRevB.3.1338.

[31] Tu CS, Chen PY, Chen CS, Lin CY and Schmidt VH. Tailoring Microstructure and Photovoltaic Effect in Multiferroic Nd-Substituted $BiFeO_3$ Ceramics by Processing Atmosphere Modification. *Journal of the European Ceramic Society*. 2018; **38**(4); 1389-1398. DOI: https://doi.org/10.1016/j.jeurceramsoc.2017.11.025.